Zero-Velocity Detection—An Algorithm Evaluation

Isaac Skog*, *Member, IEEE*, Peter Händel, *Senior Member, IEEE*, John-Olof Nilsson, and Jouni Rantakokko

***Abstract*—In this paper, we investigate the problem of detecting-time epochs when zero-velocity updates can be applied in a foot-mounted inertial navigation (motion-tracking) system. We examine three commonly used detectors: the acceleration-moving variance detector, the acceleration-magnitude detector, and the angular rate energy detector. We demonstrate that all detectors can be derived within the same general likelihood ratio test (LRT) framework, given the different prior knowledge about the sensor signals. Further, by combining all prior knowledge, we derive a new LRT detector. Subsequently, we develop a methodology to evaluate the performance of the detectors. Employing the developed methodology, we evaluate the performance of the detectors using leveled ground, slow (approximately 3 km/h) and normal (approximately 5 km/h) gait data. The test results are presented in terms of detection versus false-alarm probability. Our preliminary results show that the new detector performs marginally better than the angular rate energy detector that outperforms both the acceleration-moving variance detector and the acceleration-magnitude detector.**

***Index Terms*—Biomedical signal processing, detection, detection algorithm, inertial navigation, navigation.**

I. Introduction

THE development of low-cost miniature inertial sensors has opened up many new application fields, where traditionally the use of inertial sensors has been too costly or the sensors too bulky. Two such application fields are ambulatory gait analysis and pedestrian navigation, where the use of foot-mounted inertial sensors has shown promising results. Refer to, for example, [1]–[5] and [6]–[12], for descriptions of the usage of foot-mounted inertial sensors in pedestrian navigation and ambulatory gait analysis, respectively. This common use of foot-mounted inertial sensors has created a direct link between these research fields; researchers from both fields are now working on solving common technical challenges. In this paper, we study one of these technical challenges: how to reliably detect when zero-velocity updates can be applied to reduce the error drift of an inertial sensor-based navigation (motion-tracking) system.

Manuscript received November 8, 2009; revised Feburary 12, 2010 and June 18, 2010; accepted July 3, 2010. Date of publication July 26, 2010; date of current version October 15, 2010. *Asterisk indicates corresponding author.*

*I. Skog is with the ACCESS Linnaeus Center, Signal Processing Lab, Royal Institute of Technology, Stockholm, SE-100 44 Sweden (e-mail: isaac.skog@ee.kth.se).

P. Händel and J.-O. Nilsson are with the ACCESS Linnaeus Center, Signal Processing Lab, Royal Institute of Technology, Stockholm, SE-100 44 Sweden. (e-mail: ph@kth.se; jnil02@kth.se).

J. Rantakokko is with the Department of Communication Systems, Swedish Defense Research Agency, Linköping, SE-164 90 Sweden (e-mail: jouni.rantakokko@foi.se).

Digital Object Identifier 10.1109/TBME.2010.2060723

A. Application of Foot-Mounted Inertial Sensor Information in Gait Analysis and Pedestrian Navigation

In both ambulatory gait analysis and pedestrian navigation systems that employ foot-mounted inertial sensors, the sensor information is used to estimate the motion of the point of the foot, where the sensors are attached. However, the motion information is then used for different purposes.

In ambulatory gait analysis, motion information is generally used to extract spatial and temporal gait parameters during daily-life activities that may be used to analyze biomedical phenomena. To give a few examples, in [6] and [7], the motion information is used to calculate the center of mass displacement, the center of pressure, and the ground reaction force of a walking subject; parameters important when assessing energy expenditure and stability of human walking. In [13] and [14], the ankle and foot dynamics of a subject that is walking and running are studied using the motion information. In [12], the energy expenditure rate when walking is estimated from the motion information. In [11], the motion information is used to quantify the gait of several control subjects, with the aim of developing ambulatory gait analysis systems to detect and diagnose neurological disorders.

In pedestrian navigation systems that use foot-mounted inertial sensors [1], [4], [15], the motion dynamics of the foot during a single-gait event is of low interest. Instead, of interest are the accumulated motions of the foot over several steps. This information, when given the initial position of the user, may be used to track the user's position without the aid of any external information sources.

B. Methods Used to Bound Error Growth

Even though the motion information provided by the foot-mounted inertial sensors are used for different purposes in the gait analysis and the pedestrian navigation, both application fields require motion information of a high quality. Thus, both fields suffer from the same problem related to inertial navigation (motion tracking), i.e., the unbounded position and velocity error growth due to sensor artifacts. A rule of thumb is that for inertial navigation systems (INSs) employing low-cost sensors, the position error is proportional to the cube of the operation time. Therefore, with the performance of the low-cost inertial sensors currently available, free-inertial navigation is only feasible for time periods in the range of a few seconds [16]–[18].

However, the cubic-error growth can be reduced by imposing constraints on the navigation solution using information about the system dynamics [1], [16], [17]. A type of information commonly used for this purpose is knowledge about the time epochs when the system is in a stationary phase, i.e., when the system has a constant position and attitude. Using this information to bound the error growth is referred to as using zero-velocity

updates. Zero-velocity updates are well suited for bounding the error growth of a foot-mounted INS, as during ordinary gait the foot returns to a stationary state on a regular base [19].

How the zero-velocity updates are put into the practice differs with the application, but generally they may be classified as either "hard" or "soft" updates. In foot-mounted, inertial sensor-based pedestrian navigation systems, where the accumulated motion of the foot over several steps is of interest, "soft" zero-velocity updates are commonly used. That is, the knowledge of when the system has zero velocity is used together with a model for how the position, velocity, and attitude errors develop with time, to provide an estimate of the accumulated errors since the last zero-velocity update. The estimate of the accumulated errors is then fed back to correct the navigation solution and calibrate the navigation algorithm. Refer to [1] for details on how a "soft" zero-velocity update can be implemented.

In the gait analysis, where the motion of the foot during the individual gait cycles, but not the accumulated motion of the foot over several cycles, is of interest, "hard" zero-velocity updates are commonly used. The updates are hard in the sense that when the system imposes a zero-velocity update, the position, the velocity, and the yaw are reset to zero, and the roll and pitch are initialized directly from the accelerometer readings of the gravity acceleration. Refer to [6] for a description of how a "hard" zero-velocity update may be used to reinitialize an inertial navigation algorithm used to track the foot motion during the swing phase of the gait cycle.

C. Motivation and Paper Outline

Whether "hard" or "soft" zero-velocity updates are used, they require the identification of the time epochs when the inertial sensors are stationary. Accordingly, a range of detectors has been proposed for detecting the stationary epochs based on the inertial sensor data [2]–[4], [13], [20]–[22]. However, the proposed detectors are generally derived in an *ad hoc* manner and the literature lacks a study on their characteristics and performance. The aim of this paper is to formalize the detection problem as a hypothesis testing problem, and to use the results from the statistical-detection theory to analyze the detectors. The theoretical findings are then supported by testing the detectors on data recorded under two gait conditions.

The outline of the paper is as follows. In Section II, we mathematically formalize the detection problem and put it into a detection theory framework. Thereafter, in Section III, we define the signal and sensor model, and specify our prior knowledge about the system dynamics. In Section IV, we introduce the generalized likelihood ratio test (GLRT) [23], and use it to derive a new zero-velocity detector. Furthermore, we show that the three most commonly found detectors in the literature are special cases of the derived detector. In Section V, we evaluate the performance of the detectors. Finally, in Section VI, we summarize the results and conclusions are drawn.

II. Problem Definition

Assume that a six-degree-of-freedom inertial measurement unit (IMU), i.e., an assembly of three accelerometers and three gyroscopes, has been attached to the instep of a foot, as illustrated in Fig. 1. Let $\mathbf{y}_k \in \mathbb{R}^6$ be the vector

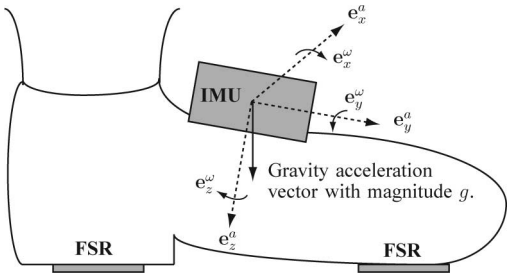

Fig. 1. Illustration of the instep-mounted IMU and the FSRs used in the reference system. The reference system is used to evaluate the performance of the detectors and is described in Section V. The measurements $\mathbf{y}_k^a$ and $\mathbf{y}_k^\omega$ are the specific force (i.e., the combined inertial and gravity acceleration) and the angular rate, experienced by the IMU at time k, projected onto the accelerometer cluster coordinate axes $\{\mathbf{e}_x^a, \mathbf{e}_y^a, \mathbf{e}_z^a\}$ and gyroscope cluster coordinate axes $\{\mathbf{e}_x^\omega, \mathbf{e}_y^\omega, \mathbf{e}_z^\omega\}$, respectively.

$$\mathbf{y}_k = \begin{bmatrix} \mathbf{y}_k^a \\ \mathbf{y}_k^\omega \end{bmatrix} \tag{1}$$

that denotes the output from the IMU, i.e., the measured specific force vector[1] $\mathbf{y}_k^a \in \mathbb{R}^3$, and the angular rate vector $\mathbf{y}_k^\omega \in \mathbb{R}^3$ at the time instant k. The objective of the zero-velocity detection is to decide whether, during a time epoch consisting of N observations[2] between the time instants n and $n+N-1$, the IMU is moving or stationary, given the measurement sequence $\mathbf{z}_n \stackrel{\triangle}{=} \{\mathbf{y}_k\}_{k=n}^{n+N-1}$. Further, the decisions should be made in such a way that the probability of deciding that the IMU is stationary when it is not should be kept low. This is owing to the ruinous effect of imposing an erroneous zero-velocity constraint on the navigation solution. However, as imposing the zero-velocity constraints when it holds true is the key to breaking the cubic-error drift, the probability of detecting the stationary events should be maximized given a certain false-alarm probability, i.e., given the probability to decide that the IMU is stationary when it is not.

Mathematically, we can formalize the detection problem as a binary hypothesis testing problem, where the detector can choose between the two hypotheses $\mathcal{H}_0$ and $\mathcal{H}_1$ defined as follows:

$$\begin{aligned} \mathcal{H}_0 &: \text{ IMU is moving} \\ \mathcal{H}_1 &: \text{ IMU is stationary.} \end{aligned} \tag{2}$$

The detector performance is then specified by the false-alarm probability, $P_{\mathrm{FA}} = \Pr\{\mathcal{H}_1|\mathcal{H}_0\}$ (i.e., the probability of deciding on the hypothesis $\mathcal{H}_1$, when hypothesis $\mathcal{H}_0$ is true) and the probability of detection $P_D = \Pr\{\mathcal{H}_1|\mathcal{H}_1\}$ (i.e., the probability

[1] An accelerometer measures the difference between the true acceleration in inertial space and the acceleration due to gravity. This quantity, i.e., the nongravitational force per unit mass exerted on the accelerometer, is commonly referred to as the "specific force" [24], [25].

[2] The choice on the number of observations N will depend upon the sample rate of the system and the length of the time epochs for which the IMU is assumed stationary.

of deciding hypothesis $\mathcal{H}_1$ when it is true). Further, Neyman–Pearson theorem tells us how to choose between the two hypotheses to maximize P_D for a given $P_{\rm FA}$. Let $p(\mathbf{z}_n;\mathcal{H}_0)$ and $p(\mathbf{z}_n;\mathcal{H}_1)$ denote the probability density functions (pdfs) of the observations for the two hypotheses. Thus, the Neyman–Pearson theorem then states that [23].

Theorem 1 (Neyman–Pearson): To maximize P_D for $P_{\rm FA} = \alpha$, decide on $\mathcal{H}_1$ if

$$L(\mathbf{z}_n) = \frac{p(\mathbf{z}_n;\mathcal{H}_1)}{p(\mathbf{z}_n;\mathcal{H}_0)} > \gamma \tag{3}$$

where the threshold γ is determined from

$$P_{\rm FA} = \int_{\{\mathbf{z}_n : L(\mathbf{z}_n)>\gamma\}} p(\mathbf{z}_n;\mathcal{H}_0)\, d\mathbf{z}_n = \alpha. \tag{4}$$

The function $L(\mathbf{z}_n)$ in (3) is referred to as the likelihood ratio, as for each value $\mathbf{z}_n$, it indicates the likelihood of the $\mathcal{H}_1$ hypothesis versus the $\mathcal{H}_0$ hypothesis. Moreover, the test in (3) is referred to as the likelihood ratio test (LRT). Clearly, the LRT requires complete knowledge about the pdfs of the observations for the two hypotheses. Therefore, as the pdfs of the observations are mostly only partly known, we often have to choose approximate hypothesis tests methods.

III. Signal and Sensor Model

The pdfs of the observed data depends both upon the true signal and the distortion introduced to the signal by the sensors. Hence, to find the pdfs of the observations, we must specify a signal and sensor model. The choice of models should be balanced between the mathematical tractability and realistic description of the signal and the sensor.

A. Sensor Model

For IMU sensors, there is a vast amount of models with various complexities [24], [26], [27]. We will restrict our analysis to the case when the IMU output may be described as follows:

$$\mathbf{y}_k = \mathbf{s}_k(\theta) + \mathbf{v}_k \tag{5}$$

where

$$\mathbf{s}_k(\theta) = \begin{bmatrix} \mathbf{s}_k^a(\theta) \\ \mathbf{s}_k^\omega(\theta) \end{bmatrix} \quad \text{and} \quad \mathbf{v}_k = \begin{bmatrix} \mathbf{v}_k^a \\ \mathbf{v}_k^\omega \end{bmatrix}. \tag{6}$$

Here, $\mathbf{s}_k^a(\theta) \in \mathbb{R}^3$ and $\mathbf{s}_k^\omega(\theta) \in \mathbb{R}^3$ denote the IMU-experienced specific force and angular rate, respectively. Further, θ denotes the set of unknown parameters needed to describe the signals. Moreover, $\mathbf{v}_k^a \in \mathbb{R}^3$ and $\mathbf{v}_k^\omega \in \mathbb{R}^3$ denote the noise associated with the accelerometer- and gyroscope-sensor assembly, respectively. We will assume that the noise is independent identically distributed zero-mean, Gaussian with covariance matrix

$$\mathbf{C} = \mathbb{E}\{\mathbf{v}_k\, \mathbf{v}_k^T\} = \begin{bmatrix} \sigma_a^2\, \mathbf{I}_3 & \mathbf{0}_3 \\ \mathbf{0}_3 & \sigma_\omega^2\, \mathbf{I}_3 \end{bmatrix} \tag{7}$$

where $\mathbf{I}_3$ ($\mathbf{0}_3$) denotes an identity (zero) matrix of size 3×3, and T denotes the transpose operation. Further, $\mathbb{E}\{\cdot\}$ denotes the expectation operation, and $\sigma_a^2 \in \mathbb{R}^1$ and $\sigma_\omega^2 \in \mathbb{R}^1$ denote the accelerometer and gyroscope noise variance, respectively.

B. Signal Model

Modeling the specific force and angular rates, i.e., $\mathbf{s}_k(\theta)$ experienced by the foot-mounted IMU under the hypothesis $\mathcal{H}_0$ (that the IMU is in motion) in a consistent way that reflects a diverse set of gaits, is difficult. However, under the hypothesis $\mathcal{H}_1$ (that the IMU is stationary), the following conditions hold true.

1) The specific force measured by the accelerometers assembly is only due to the ground's standoff to the gravitation acceleration, whose magnitude is known.
2) The attitude of the IMU is constant, i.e., the angular rate experienced by the IMU is zero.

In other words, mathematically, for the two hypotheses, the signal fulfills the conditions

$$\begin{aligned} \mathcal{H}_0 &: \exists\, k \in \Omega_n \ \text{ s.t. } \mathbf{s}_k^a(\theta) \neq g\mathbf{u}_n \ \text{ or } \ \mathbf{s}_k^\omega(\theta) \neq \mathbf{0}_{3,1} \\ \mathcal{H}_1 &: \forall k \in \Omega_n \ \text{ then } \ \mathbf{s}_k^a(\theta) = g\mathbf{u}_n \ \text{ and } \ \mathbf{s}_k^\omega(\theta) = \mathbf{0}_{3,1}. \end{aligned} \tag{8}$$

Here, $\mathbf{u}_n \in \Omega_u$, where $\Omega_u = \{\mathbf{u} \in \mathbb{R}^3 : \|\mathbf{u}\| = 1\}$ and $g \in \mathbb{R}^1$ is the magnitude of the local gravity vector. Moreover, $\|\mathbf{u}\| = \sqrt{\mathbf{u}^T\, \mathbf{u}}$ and $\Omega_n = \{\ell \in \mathbb{N} : n \leq \ell < N-1\}$. Hence, for the two hypothesis, the unknown parameters of the signal are as follows:

$$\begin{aligned} \mathcal{H}_0 &: \theta \equiv \{\mathbf{s}_k\}_{k=n}^{n+N-1} \\ \mathcal{H}_1 &: \theta \equiv \mathbf{u}_n. \end{aligned} \tag{9}$$

That is, under $\mathcal{H}_0$, the signal $\mathbf{s}_k(\theta)$ is completely unknown, whereas under $\mathcal{H}_1$, only the direction of the specific force vector is unknown.

C. PDFs of Observed Signals

Owing to the lack of knowledge about the signal parameters θ, we cannot completely specify the pdfs of the observations under the two hypotheses. However, with the sensor model specified by (5)–(7), the measurements may originate from the family of pdfs, which are given by (for $i = 0, 1$)

$$\begin{aligned} p(\mathbf{z}_n;\theta,\mathcal{H}_i) &= \prod_{k\in\Omega_n} p(\mathbf{y}_k;\theta,\mathcal{H}_i) \\ &= \prod_{k\in\Omega_n} p(\mathbf{y}_k^a;\theta,\mathcal{H}_i)\, p(\mathbf{y}_k^\omega;\theta,\mathcal{H}_i) \end{aligned} \tag{10}$$

where

$$p(\mathbf{y}_k^a;\theta,\mathcal{H}_i) = \frac{1}{(2\pi\sigma_a^2)^{3/2}}\, \exp\left(-\frac{1}{2\sigma_a^2}\|\mathbf{y}_k^a - \mathbf{s}_k^a(\theta)\|^2\right) \tag{11}$$

and

$$p(\mathbf{y}_k^\omega;\theta,\mathcal{H}_i) = \frac{1}{(2\pi\sigma_\omega^2)^{3/2}}\, \exp\left(-\frac{1}{2\sigma_\omega^2}\|\mathbf{y}_k^\omega - \mathbf{s}_k^\omega(\theta)\|^2\right). \tag{12}$$

IV. Generalized Likelihood Rate Tests

As the pdfs of the observations under the two hypotheses are parameterized by a set of, to us, unknown parameters θ, i.e., the (partly) unknown signal $\mathbf{s}_k(\theta)$, we cannot apply the LRT in (3).

However, by substituting the unknown parameters with their maximum likelihood estimates (MLEs) [28], we can derive a GLRT. The GLRT decides on $\mathcal{H}_1$, if

$$L_G(\mathbf{z}_n) = \frac{p(\mathbf{z}_n; \hat{\theta}^1, \mathcal{H}_1)}{p(\mathbf{z}_n; \hat{\theta}^0, \mathcal{H}_0)} > \gamma \tag{13}$$

where $\hat{\theta}^1$ is the MLE of the unknown parameters assuming $\mathcal{H}_1$ is true, and $\hat{\theta}^0$ is the MLE of the unknown parameters assuming $\mathcal{H}_0$ is true.

The MLE is obtained by maximizing (10) with respect to the unknown parameters. In our case, under $\mathcal{H}_0$, the signal is completely unknown and $\hat{\theta}^0 = \{\mathbf{y}_k\}_{k=n}^{n+N-1}$. Thus,

$$p(\mathbf{z}_n; \hat{\theta}^0, \mathcal{H}_0) = \frac{1}{(2\pi\sigma_a^2)^{3\,N/2}} \cdot \frac{1}{(2\pi\sigma_\omega^2)^{3\,N/2}}. \tag{14}$$

Under $\mathcal{H}_1$, we can obtain the MLE of the unknown signal parameter $\mathbf{u}_n$ by maximizing

$$p(\mathbf{z}_n; \mathbf{u}_n, \mathcal{H}_1) = \frac{1}{(2\pi\sigma_a^2)^{3\,N/2}} \exp\left(-\frac{1}{2\sigma_a^2} \sum_{k\in\Omega_n} \|\mathbf{y}_k^a - g\mathbf{u}_n\|^2\right) \cdot \frac{1}{(2\pi\sigma_\omega^2)^{3\,N/2}} \exp\left(-\frac{1}{2\sigma_\omega^2} \sum_{k\in\Omega_n} \|\mathbf{y}_k^\omega\|^2\right) \tag{15}$$

with respect to $\mathbf{u}_n \in \Omega_u$. That is,

$$\begin{aligned}\hat{\mathbf{u}}_n &= \arg\max_{\mathbf{u}\in\Omega_u}(p(\mathbf{z}_n; \mathbf{u}, \mathcal{H}_1)) \\ &= \arg\min_{\mathbf{u}\in\Omega_u}\left(\sum_{k\in\Omega_n} \|\mathbf{y}_k^a - g\mathbf{u}\|^2\right) \\ &= \arg\min_{\mathbf{u}\in\Omega_u}\left(\sum_{k\in\Omega_n} \|\mathbf{y}_k^a\|^2 - 2\,g(\mathbf{y}_k^a)^T\mathbf{u} + g^2\|\mathbf{u}\|^2\right) \\ &= \arg\max_{\mathbf{u}\in\Omega_u}((\overline{\mathbf{y}}_n^a)^T\mathbf{u}) = \frac{\overline{\mathbf{y}}_n^a}{\|\overline{\mathbf{y}}_n^a\|}\end{aligned} \tag{16}$$

where

$$\overline{\mathbf{y}}_n^a = \frac{1}{N}\sum_{k\in\Omega_n} \mathbf{y}_k^a. \tag{17}$$

The last equality in (16) follows from Cauchy's Schwarz inequality $\mathbf{a}^T\mathbf{b} \le \|\mathbf{a}\|\|\mathbf{b}\|$, with equality observed only if $\mathbf{a} = c\,\mathbf{b}$; c is a real constant. Substituting $\hat{\mathbf{u}}_n$ into (15) yields

$$\begin{aligned}p(\mathbf{z}_n; \hat{\theta}^1, \mathcal{H}_1) &= p(\mathbf{z}_n; \hat{\mathbf{u}}_n, \mathcal{H}_1) \\ &= \frac{1}{(2\pi\sigma_a^2)^{3\,N/2}} \cdot \frac{1}{(2\pi\sigma_\omega^2)^{3\,N/2}} \\ &\quad \cdot \exp\left(-\frac{1}{2\sigma_a^2}\sum_{k\in\Omega_n}\left\|\mathbf{y}_k^a - g\frac{\overline{\mathbf{y}}_n^a}{\|\overline{\mathbf{y}}_n^a\|}\right\|^2\right) \\ &\quad \cdot \exp\left(-\frac{1}{2\sigma_\omega^2}\sum_{k\in\Omega_n}\|\mathbf{y}_k^\omega\|^2\right).\end{aligned} \tag{18}$$

Next, if we combine (13), (14), and (18), the GLRT becomes: decide on $\mathcal{H}_1$ if

$$L_G(\mathbf{z}_n) = \exp\left(-\frac{1}{2\sigma_a^2}\sum_{k\in\Omega_n}\left\|\mathbf{y}_k^a - g\frac{\overline{\mathbf{y}}_n^a}{\|\overline{\mathbf{y}}_n^a\|}\right\|^2\right) \cdot \exp\left(-\frac{1}{2\sigma_\omega^2}\sum_{k\in\Omega_n}\|\mathbf{y}_k^\omega\|^2\right) > \gamma. \tag{19}$$

We may further simplify the test with respect to the fact that the logarithm is monotonically increasing. To do so, let

$$T(\mathbf{z}_n) = -\frac{2}{N}\ln L_G(\mathbf{z}_n). \tag{20}$$

We can then state the GLRT as: choose $\mathcal{H}_1$ if

$$T(\mathbf{z}_n) = \frac{1}{N}\sum_{k\in\Omega_n}\left(\frac{1}{\sigma_a^2}\left\|\mathbf{y}_k^a - g\frac{\overline{\mathbf{y}}_n^a}{\|\overline{\mathbf{y}}_n^a\|}\right\|^2 + \frac{1}{\sigma_\omega^2}\|\mathbf{y}_k^\omega\|^2\right) < \gamma' \tag{21}$$

where $\gamma' = -(2/N)\ln(\gamma)$. We can interpret this as follows: if the mean square error of fitting a vector of magnitude g with the direction of the average specific force vector to the accelerometer data in combination with the energy in the gyroscope signal, each weighted by the quality of the measurements, falls below the threshold γ', the GLRT chooses the hypothesis that the IMU is stationary. The new detector defined by the GLRT in (21) will for simplicity, throughout the paper, be referred to as the stance hypothesis optimal detection (SHOE) detector.

A. Acceleration-Moving Variance Detector

A detector proposed in the literature to detect when the IMU is stationary, is the acceleration-moving variance detector [2], [13], [20], [21]. The moving variance detector is solely based upon the accelerometer data and is defined as follows: decide on $\mathcal{H}_1$ if

$$T_v(\mathbf{z}_n^a) = \frac{1}{N}\sum_{k\in\Omega_n}\|\mathbf{y}_k^a - \overline{\mathbf{y}}_n^a\|^2 < \gamma_v \tag{22}$$

where $\mathbf{z}_n^a \triangleq \{\mathbf{y}_k^a\}_{k=n}^{n+N-1}$. We can derive the acceleration-moving variance detector within the GLRT framework considering the fact that the orientation of the accelerometer assembly is constant when the IMU is stationary, but neglecting the fact that the magnitude of the specific force vector is equal to g. To derive the test, let us assume that under the two hypotheses, the signal from the accelerometer cluster fulfills the conditions

$$\begin{aligned}\mathcal{H}_0 &: \exists\, k \in \Omega_n \ \text{ s.t. } \ \mathbf{s}_k^a(\theta_v) \neq \mathbf{s}^a \\ \mathcal{H}_1 &: \forall k \in \Omega_n \ \text{ then } \ \mathbf{s}_k^a(\theta_v) = \mathbf{s}^a\end{aligned} \tag{23}$$

where $\mathbf{s}^a \in \mathbb{R}^3$ is unknown. Hence, the unknown parameters needed to describe the signal under the two hypotheses are as follows:

$$\begin{aligned}\mathcal{H}_0 &: \theta_v \equiv \{\mathbf{s}_k^a\}_{k=n}^{n+N-1} \\ \mathcal{H}_1 &: \theta_v \equiv \mathbf{s}^a\end{aligned} \tag{24}$$

and thus, the family of pdfs describing the accelerometer observations is given by (for $i = 0, 1$)

$$p(\mathbf{z}_n^a; \theta_v, \mathcal{H}_i) = \prod_{k \in \Omega_n} p(\mathbf{y}_k^a, \theta_v, \mathcal{H}_i). \tag{25}$$

With this information in hand, under $\mathcal{H}_0$, the MLE, $\hat{\theta}_v^0 = \{\mathbf{y}_k^a\}_{k=n}^{n+N-1}$. Thus,

$$p(\mathbf{z}_n^a; \hat{\theta}_v^0, \mathcal{H}_0) = \frac{1}{(2\pi\sigma_a^2)^{3N/2}}. \tag{26}$$

Further, the MLEs of the unknown parameters under $\mathcal{H}_1$ are given by

$$\begin{aligned} \hat{\mathbf{s}}^a &= \arg\max_{\mathbf{s}} (p(\mathbf{z}_n^a; \mathbf{s}, \mathcal{H}_1)) \\ &= \arg\min_{\mathbf{s}} \left(\sum_{k \in \Omega_n} \|\mathbf{y}_k^a - \mathbf{s}\|^2 \right) = \overline{\mathbf{y}}_n^a. \end{aligned} \tag{27}$$

Therefore,

$$\begin{aligned} p(\mathbf{z}_n^a; \hat{\theta}_v^1, \mathcal{H}_1) = p(\mathbf{z}_n^a; \hat{\mathbf{s}}^a, \mathcal{H}_1) &= \frac{1}{(2\pi\sigma_a^2)^{3N/2}} \\ &\cdot \exp\left(-\frac{1}{2\sigma_a^2} \sum_{k \in \Omega_n} \|\mathbf{y}_k^a - \overline{\mathbf{y}}_n^a\|^2 \right). \end{aligned} \tag{28}$$

Hence, if we combine (13), (20), (26), and (28), the GLRT becomes: choose $\mathcal{H}_1$ if

$$\begin{aligned} T_v'(\mathbf{z}_n^a) &= -\frac{2}{N} \ln \frac{p(\mathbf{z}_n^a; \hat{\theta}_v^1, \mathcal{H}_1)}{p(\mathbf{z}_n^a; \hat{\theta}_v^0, \mathcal{H}_0)} \\ &= \frac{1}{\sigma_a^2 N} \sum_{k \in \Omega_n} \|\mathbf{y}_k^a - \overline{\mathbf{y}}_n^a\|^2 < \gamma_v' \end{aligned} \tag{29}$$

which is equivalent to the test in (22).

B. Acceleration-Magnitude Detector

The acceleration-magnitude detector is another detector proposed in the literature [2], [21], [22], and is often used as a supplement to the moving variance detector. The acceleration-magnitude detector checks if the measured specific force vector is close to g, and if that is the case, concludes that the IMU is stationary. We can derive this type of detector within the GLRT framework based on the fact that the magnitude of the specific force vector is g when the IMU is stationary, but neglecting the fact that the direction of the vector should be constant. To derive the test, let us assume that under the two hypotheses, the signal from the accelerometer cluster fulfills the conditions

$$\begin{aligned} \mathcal{H}_0 &: \exists\, k \in \Omega_n \ \text{ s.t. } \ \mathbf{s}_k^a(\theta_m) \neq g\mathbf{u}_k \\ \mathcal{H}_1 &: \forall k \in \Omega_n \ \text{ then } \ \mathbf{s}_k^a(\theta_m) = g\mathbf{u}_k \end{aligned} \tag{30}$$

where $\mathbf{u}_k \in \Omega_u$. Hence, the unknown parameters needed to describe the signal under the two hypotheses are as follows:

$$\begin{aligned} \mathcal{H}_0 &: \theta_m \equiv \{\mathbf{s}_k^a\}_{k=n}^{n+N-1} \\ \mathcal{H}_1 &: \theta_m \equiv \{\mathbf{u}_k\}_{k=n}^{n+N-1}. \end{aligned} \tag{31}$$

Again, the family of pdfs describing the accelerometer observations is given by (25); however, now the unknown parameters are those in (31). Under $\mathcal{H}_0$, when the signal is completely unknown, the MLEs $\hat{\theta}_m^0 = \{\mathbf{y}_k^a\}_{k=n}^{n+N-1}$ and $p(\mathbf{z}_n^a; \hat{\theta}_m^0, \mathcal{H}_0)$ are given by (26). Further, under $\mathcal{H}_1$, the MLEs of the unknown parameters are given by (for $\ell = n, \ldots, N+n-1$)

$$\begin{aligned} \hat{\mathbf{u}}_\ell &= \arg\max_{\mathbf{u}_\ell \in \Omega_u} \left(p(\mathbf{z}_n^a; \{\mathbf{u}_k\}_{k=n}^{n+N-1}, \mathcal{H}_1) \right) \\ &= \arg\min_{\mathbf{u}_\ell \in \Omega_u} \left(\sum_{k \in \Omega_n} \|\mathbf{y}_k^a - g\,\mathbf{u}_k\|^2 \right) \\ &= \arg\min_{\mathbf{u}_\ell \in \Omega_u} \left(\|\mathbf{y}_\ell^a - g\,\mathbf{u}_\ell\|^2 \right) = \frac{\mathbf{y}_\ell^a}{\|\mathbf{y}_\ell^a\|}. \end{aligned} \tag{32}$$

Thus,

$$\begin{aligned} p(\mathbf{z}_n; \hat{\theta}_m^1, \mathcal{H}_1) &= p(\mathbf{z}_n; \{\hat{\mathbf{u}}_k\}_{k=n}^{n+N-1}, \mathcal{H}_1) \\ &= \frac{1}{(2\pi\sigma_a^2)^{3\,N/2}} \\ &\cdot \exp\left(-\frac{1}{2\sigma_a^2} \sum_{k \in \Omega_n} \left\| \mathbf{y}_k^a - g \frac{\mathbf{y}_k^a}{\|\mathbf{y}_k^a\|} \right\|^2 \right). \end{aligned} \tag{33}$$

Hence, if we combine (13), (20), (26), and (33), the GLRT becomes as follows: choose $\mathcal{H}_1$, if

$$T_m(\mathbf{z}_n^a) < \gamma_m \tag{34}$$

where

$$\begin{aligned} T_m(\mathbf{z}_n^a) &= -\frac{2}{N} \ln \frac{p(\mathbf{z}_n^a; \hat{\theta}_m^1, \mathcal{H}_1)}{p(\mathbf{z}_n^a; \hat{\theta}_m^0, \mathcal{H}_0)} \\ &= \frac{1}{\sigma_a^2 N} \sum_{k \in \Omega_n} \left\| \mathbf{y}_k^a - g \frac{\mathbf{y}_k^a}{\|\mathbf{y}_k^a\|} \right\|^2 \\ &= \frac{1}{\sigma_a^2 N} \sum_{k \in \Omega_n} (\|\mathbf{y}_k^a\| - g)^2. \end{aligned} \tag{35}$$

C. Angular Rate Energy Detector

Sometimes, only the energy in the gyroscope signal is used to detect when the IMU is stationary [3], [4], [29]. The angular rate energy detector decides on $\mathcal{H}_1$ if

$$T_\omega(\mathbf{z}_n^\omega) = \frac{1}{N} \sum_{k \in \Omega_n} \|\mathbf{y}_k^\omega\|^2 < \gamma_\omega \tag{36}$$

where $\mathbf{z}_n^\omega \triangleq \{\mathbf{y}_k^\omega\}_{k=n}^{n+N-1}$. The test statistics $T_\omega(\mathbf{z}_n^\omega)$ correspond to the last part of the GLRT statistics in (20), except for the scaling with σ_ω^2. Thus, we can also derive the angular rate energy detector within the GLRT framework.

Worth noting is that the actual values of the noise variances σ_a^2 and σ_ω^2 have no influence on the performance of the acceleration-moving variance detector, the acceleration-magnitude detector, and the angular rate energy detector. The noise variances only scale the test statistics. However, for the SHOE detector, the ratio between the noise variances, that is $\sigma_a^2/\sigma_\omega^2$, affects the performance of the detector; the ratio reflects the disturbances in

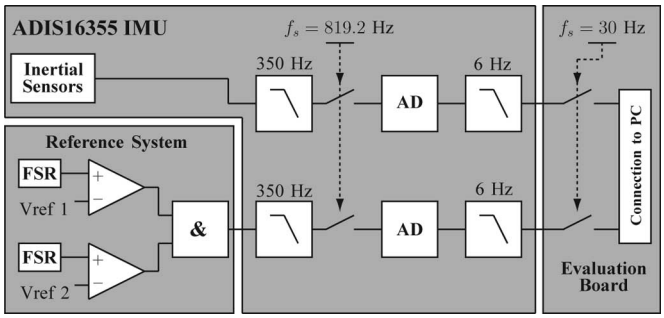

Fig. 2. Block diagram of the inertial sensors and reference system. The resistance of the FSRs are compared to the thresholds defined by Vref 1 and Vref 2, respectively. The outputs of the comparators are inserted to a logical AND gate, whose output is sampled simultaneously with the inertial sensors at rate of 819.2 Hz. The signals are then passed through the digital low-pass filters of the ADIS16355, before they are down sampled to 30 Hz and transmitted to the PC by the ADIS16355 evaluation board.

the information from the accelerometers versus the disturbances in the information from the gyroscopes. Further, we may note that the angular rate energy detector is a special case of the SHOE detector arising when $\sigma_a^2/\sigma_\omega^2 \to \infty$.

V. Performance Evaluation

To evaluate the GLRT detectors examined in Section IV, we collected the gait data from an instep-mounted IMU. The IMU, an Analog Devices ADIS16355, was mounted on the instep of the user's right foot, with the coordinate axis illustrated in Fig. 1. We asked the user, a 28-year-old male with a height of 1.76 m and a weight of 67 kg, to repeatedly walk on leveled ground, a predefined rectangular trajectory; the rectangular trajectory had side lengths of 6 and 48 m, respectively. The user was first told to walk slowly (approximately 3 km/h) for 30 min, and then at normal speed (approximately 5 km/h) for another 30 min. The gait speed was controlled by telling the user his average walking speed for each lap and asking him to speed up or slow down. Two datasets were obtained, with data recorded at a sample rate of 30 Hz, corresponding to slow and normal forward gait, respectively.

The reason for using a sampling frequency of 30 Hz was due to the limitation in the data transfer rate between the evaluation board, used with the ADIS16355 IMU and the PC that stored the data. The IMU itself samples its sensors at a frequency of 819.2 Hz. To avoid aliasing effects from the down sampling to 30 Hz, the digital signals were low-pass filtered using the internal filters of the ADIS16355. Fig. 2 shows a block diagram of the sensor system.

The test statistics $T(\mathbf{z}_n)$, $T_v(\mathbf{z}_n^a)$, $T_m(\mathbf{z}_n^a)$, and $T_\omega(\mathbf{z}_n^\omega)$, when calculated for a small part of the slow-gait dataset, is shown in Fig. 3. Fig. 3 also shows the time instants n, when all the data samples in $\mathbf{z}_n^\omega$ originate from a stationary phase according to the reference system. The reference system is described in the following.

A. Reference System

As a reference system indicating when the IMU was stationary, we first considered the possibility of using an optical-tracking system. However, an optical-tracking system only works in a limited area, and therefore, is not suitable for collecting the amount of data needed to calculate reliable performance statistics for the detectors. We, therefore, constructed an ambulatory reference system out of two switches mounted beneath the heel and front sole of the user's right SHOE. This is illustrated in Fig. 1. The switches were constructed around force-sensitive resistors (FSRs) in an approach similar to that in [30]. That is, the voltage across the FSR, which varies with the force applied to the resistor, is compared to a reference voltage by a comparator; the reference voltage determines the force needed to change the state of the switch. The outputs of the two switches were then connected to a logical AND gate, whose output was sampled simultaneously with the IMU sensors using the spare analog-to-digital converter of the ADIS16355. Fig. 2 shows a block diagram of the system.

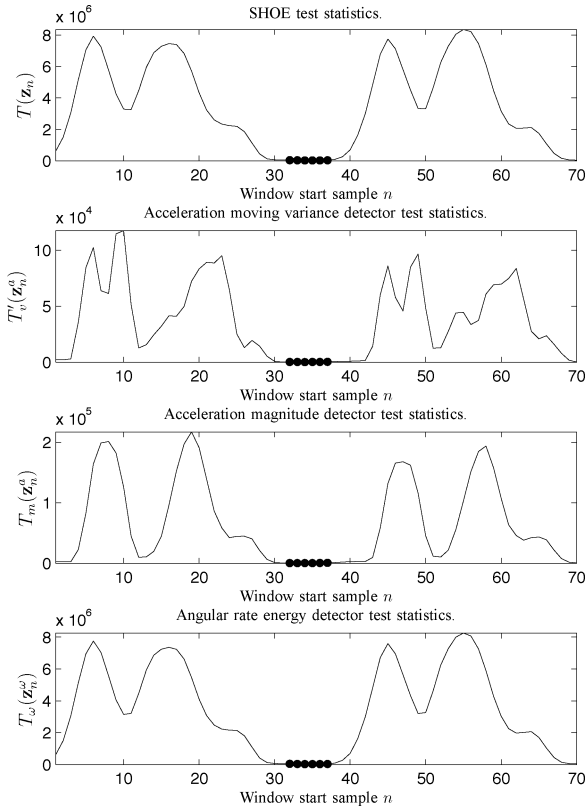

Fig. 3. Test statistics $T(\mathbf{z}_n)$, $T_v'(\mathbf{z}_n^a)$, $T_m(\mathbf{z}_n^a)$, and $T_\omega(\mathbf{z}_n^\omega)$ as a function of n for a window size $N = 5$ during slow forward gait. The dots indicate the moments n, when all data samples in $\mathbf{z}_n$ originate from a phase when the IMU was stationary according to the reference system.

The reference system thus works by the idea that if large enough forces are sensed by both switches simultaneously, then both the heel and front sole of the user's SHOE is in contact with the ground and the instep-mounted IMU is stationary. However, since neither the SHOE nor the foot of the user is a full rigid body, the assumption that the IMU is stationary only holds approximately. Several factors influence the validity of the assumption: the rigidness of the SHOE and the pronation/supination of the user, the placement of the IMU on the instep, the placement

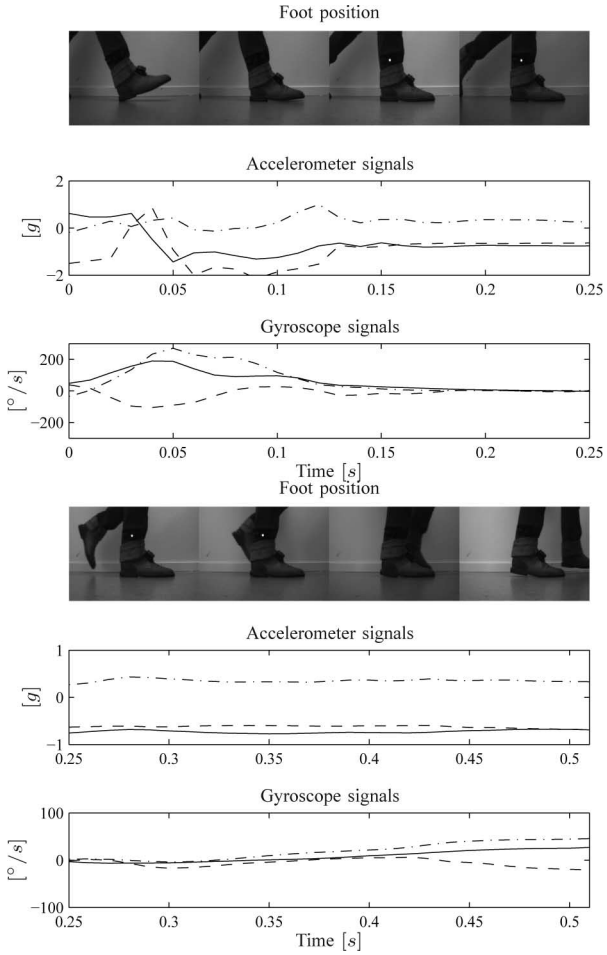

Fig. 4. Stance phase as a function of time together with the output from the accelerometers and gyroscopes. When the LED is ON (white dot in the pictures), the reference system classifies the IMU as stationary. Legend: (−·) *x*-axis, (− −) *y*-axis, and (——) *z*-axis.

of the FSRs beneath the heel and front-sole, and the threshold settings of the switches.

To minimize the effect of these factors, we calibrated our reference system by recording, with a video camera that was time synchronized to the IMU data logger, the motion of the IMU, the state of the reference system, and the output from the IMU during a single step. Based upon the recorded data, the placement of the switches and their thresholds were then adjusted and a new step recorded. The process was repeated until a satisfactory agreement was achieved between the state indicated by the reference system and the motion of the IMU in the recorded data. The final result can be seen in Fig. 4. It should be noted that in Fig. 4, every second picture frame in the recorded video has been left out.

To summarize, the reference system is not an ideal reference system and the 30-Hz sample rate is on the lower end for the application. Therefore, the results presented next should be viewed as preliminary, which should be verified by further tests. However, the results show that the presented test methodology is applicable and can be used to evaluate the detectors.

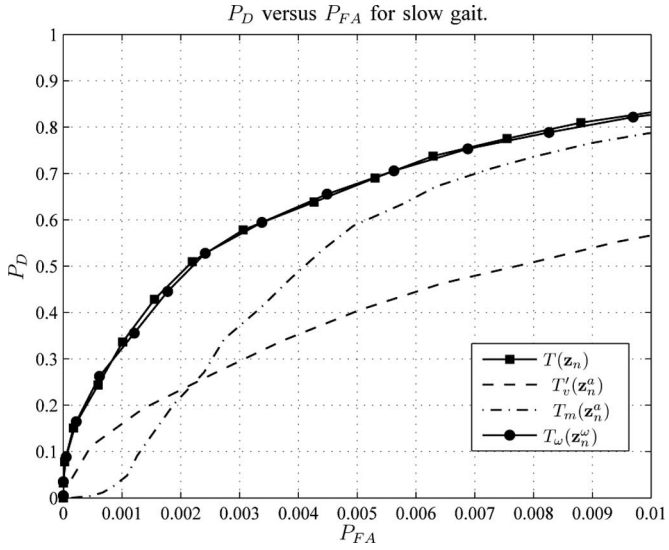

Fig. 5. Probability of detection versus probability of false alarm for the GLRT algorithms based on the slow-gait data.

B. Detector Statistics

Having collected the data, we calculated the detection and false-alarm probabilities for the detectors using a data window size[3] $N = 5$ (i.e., 150 ms) and with the noise standard deviations[4] set to $\sigma_a = 0.02\,\mathrm{m/s^2}$ and $\sigma_\omega = 0.1\,^\circ/\mathrm{s}$, respectively. That is, the receiver operating characteristics (ROC) of the detectors were calculated by varying the thresholds of the detectors and comparing the decisions of the detectors to the output of the reference system. Refer to [31] for details on how to calculate and interpret ROC curves. The calculated ROC curves for slow and normal gait are shown in Figs. 5 and 6, respectively. From Figs. 5 and 6, we can see that:

1) the angular rate energy detector and the SHOE detector have the highest performance, and behave basically in the same manner, indicating that the gyroscope signal holds the most reliable information for stationarity detection;
2) there is a significant difference in the performance of the detectors for slow- and normal-gait speed, respectively.

At first glance, it may seem that the performance of the detectors is far from efficient for any zero-velocity constrained navigation application. However, the P_D versus P_{FA} figures are partly misleading for our application. For a zero-velocity-constrained INS, it is better to have short periods of zero-velocity updates on a regular basis and let the detector work at a low P_{FA} level, rather than trying to detect all the samples in the time epoch when the IMU is stationary at the cost of a high P_{FA} level. Thus, if the detector's threshold is adjusted to a lower P_{FA} level, but the detector is still capable of detecting that the IMU is stationary at least once for most gait cycles, then the

[3]The data window size was selected by looking at the histogram of the lengths of the stationary phases according to the reference system. The histogram showed that the IMU was stationary for five or more samples during most gait cycles.

[4]The noise variance values were estimated from two minutes of data; data recorded with the IMU stationary on a table.

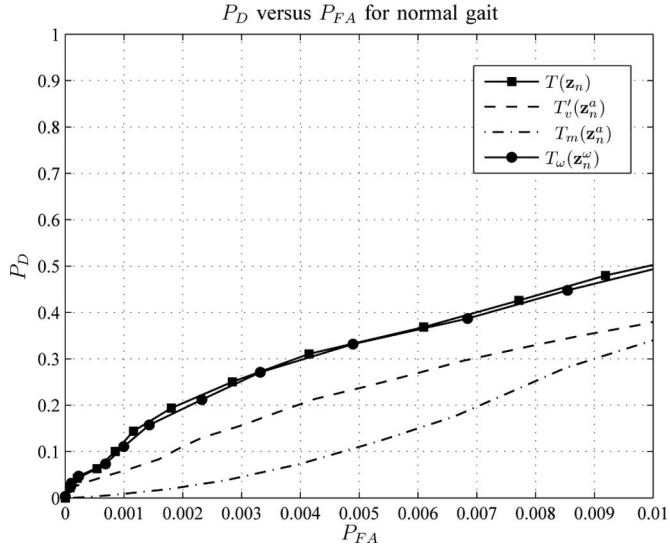

Fig. 6. Probability of detection versus probability of false alarm for the GLRT algorithms based on the normal-gait data.

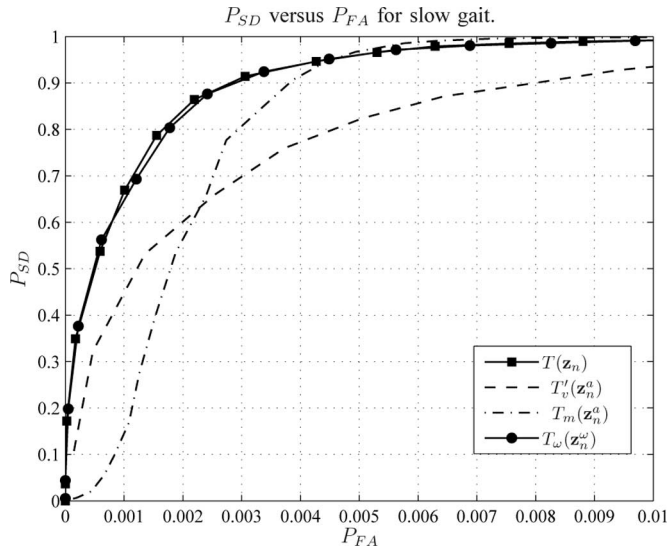

Fig. 7. Probability of stationarity detection versus probability of false alarm for the GLRT algorithms based on the slow-gait data.

periods of free-inertial navigation will be sufficiently short to avoid large error drifts.

A better measure of the performance of zero-velocity detectors is the probability of detecting at least once that the IMU is stationary in the "IMU stationary" part of the gait cycle. We, therefore, introduced the measure probability of stationarity detection P_{SD} that denotes the probability that the detector decides on $\mathcal{H}_1$ at least once in the "IMU stationary" part of the gait cycle. By recalculating the statistics of the detector in terms of P_{SD} using the datasets previously employed, we obtained the results for slow and normal gait. These are shown in Figs. 7 and 8, respectively. From Figs. 7 and 8, we can conclude that:

1) for slow gait at low P_{FA} values, the angular rate energy detector and the SHOE detector still have the highest performance, whereas for high P_{FA} values, the magnitude detector has the best performance;

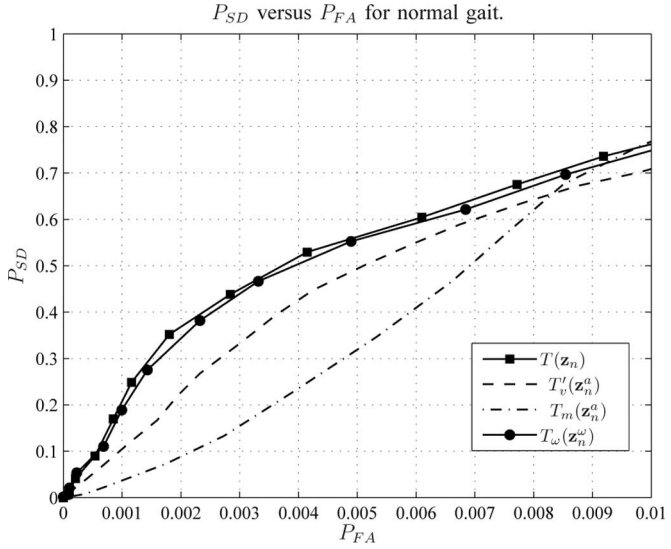

Fig. 8. Probability of stationarity detection versus probability of false alarm for the GLRT algorithms based on the normal-gait data.

2) at a normal gait speed, the SHOE detector is marginally better than the angular rate energy detector outperforming the other detector for all P_{FA} values.

The results in Figs. 5–8 indicate that the gyroscope measurements hold the most reliable information for zero-velocity detection under the experimental conditions stated, and that the accelerometer measurements only bring marginal additional information. This can also be observed from Fig. 3, where the test statistics of the acceleration-moving variance detector and the acceleration-magnitude detector are an order of magnitude smaller than those of the angular rate energy detector and the SHOE detector. We have identified two possible reasons for this: 1) the signal-to-noise ratios in the signals from gyroscopes are higher than the signal-to-noise ratios in the signals from the accelerometers and 2) there is more knowledge about the signals from the gyroscopes than about the signals from the accelerometers under the hypothesis that the IMU is stationary. The gyroscope signals we know are zero when the IMU is stationary, whereas the accelerometer signals we only know that they are constant and that the sum of their squared magnitudes is equal to g^2. Further, the fact that the test statistics of the angular rate energy detector and the SHOE detector shown in Fig. 3 are virtually identical explains why the two detectors have a similar behavior. Still, there may be other types of gait, such as uphill and downhill walking, sidestepping, and stair climbing, where the SHOE detector, which uses information from both the accelerometers and the gyroscopes, may turn out to have a superior performance. Under all circumstances, the SHOE detector should as long as the ratio $\sigma_a^2/\sigma_\omega^2$ is correctly set, theoretically, never perform worse than the other detectors, since it uses the information from all six sensors and the most complete prior information about the sensor signals.

VI. Conclusion

We investigated the problem of detecting the time epochs when zero-velocity updates are applied in a foot-mounted pedestrian navigation system. We looked at three commonly used

detectors in the literature: the acceleration-moving variance detector, the acceleration-magnitude detector, and the angular rate energy detector. We showed that all detectors can be derived within the same GLRT framework, given different prior knowledge about the sensor signals. Further, by combining all prior knowledge, we derived a new GLRT detector, referred to as the SHOE detector. We, subsequently, evaluated the performance of the detectors using slow (approximately 3 km/h) and normal (approximately 5 km/h), leveled ground, and forward-gait data. As a reference system, indicating when the IMU was stationary, we used FSRs mounted beneath the foot of the user. The test results were presented in terms of the detection versus false-alarm probability. Moreover, we calculated the probability of detecting at least once that the IMU is stationary in "IMU stationary" part of the gait cycle. This probability, being a function of the false-alarm probability, is often a better figure of merit for zero-velocity detectors used in constrained INSs.

The results show that the SHOE detector performs similarly to the angular rate energy detector [3], [4], which outperforms both the acceleration-moving variance detector [2], [13], [20], [21] and the acceleration-magnitude detector [2], [21], [22]. This indicates that the gyroscope signals hold the most reliable information for zero-velocity detection under the experimental conditions stated in this paper. Further, the results show that the performance varies between slow and normal gait, where for the latter, the proper work of the detectors is questionable.

In the literature, there are few discussions about the performance of accelerometer-based detectors versus ones based on gyroscope signals. The majority of the works considers the former class of methods. A reason for this could be that inexpensive off-the-shelf accelerometers were available on the market some years before the gyroscopes were. For instance, analog devices launched their first off-the-shelf accelerometer in the beginning of the 1990s, but their first gyroscope did not hit the market until a decade later. Nowadays, six-degrees-of-freedom IMUs are readily available, which opens the field up for detectors utilizing all 6-D. We have shown that under the given assumptions, gyroscope-based detection clearly outperforms accelerometer-based detection, and that there is no significant improvement of the detector using both accelerometer and gyroscope data, over the one that only employs signals from the gyroscopes.

REFERENCES

[1] E. Foxlin, "Pedestrian tracking with SHOE-mounted inertial sensors," *IEEE Comput. Graph. Appl.*, vol. 25, no. 6, pp. 38–46, Nov./Dec. 2005.

[2] S. Godha and G. Lachapelle, "Foot mounted inertial system for pedestrian navigation," *Meas. Sci. Technol.*, vol. 19, pp. 1–9, Jul. 2008.

[3] R. Feliz, E. Zalama, and J. G. Garcia-Bermejo, "Pedestrian tracking using inertial sensors," *J. Phys. Agents*, vol. 3, pp. 35–43, Jan. 2009.

[4] L. Ojeda and J. Borenstein, "Non-GPS navigation for security personnel and first responders," *J. Navigat.*, vol. 60, no. 3, pp. 391–407, 2007.

[5] P. Strömbäck, J. Rantakokko, S.-L. Wirkander, M. Alexandersson, I. Fors, I. Skog, and P. Händel, "Foot-mounted inertial navigation and cooperative sensor fusion for indoor positioning," in *Proc. ION 2010 Int. Tech. Meeting*, San Diego, CA, Jan.

[6] H. M. Schepers, H. F. J. M. Koopman, and P. H. Veltink, "Ambulatory assessment of ankle and foot dynamics," *IEEE Trans. Biomed. Eng.*, vol. 54, no. 5, pp. 895–902, May 2007.

[7] H. M. Schepers, E. van Asseldonk, J. H. Buurke, and P. H. Veltink, "Ambulatory estimation of center of mass displacement during walking," *IEEE Trans. Biomed. Eng.*, vol. 56, no. 4, pp. 1189–1195, Apr. 2009.

[8] A. M. Sabatini, C. Martelloni, S. Scapellato, and F. Cavallo, "Assessment of walking features from foot inertial sensing," *IEEE Trans. Biomed. Eng.*, vol. 52, no. 3, pp. 486–494, Mar. 2005.

[9] S. Bamberg, A. Y. Benbasat, D. M. Scarborough, D. E. Krebs, and J. A. Paradiso, "Gait analysis using a SHOE-integrated wireless sensor system," *IEEE Trans. Inf. Technol. Biomed.*, vol. 12, no. 4, pp. 413–423, Jul. 2008.

[10] J. M. Jasiewicz, J. H. J. Allum, J. W. Middleton, A. Barriskill, P. Condie, B. Purcell, and R. Che Tin Li, "Gait event detection using linear accelerometers or angular velocity transducers in able-bodied and spinal-cord injured individuals," *Gait Posture*, vol. 24, no. 4, pp. 502–509, 2006.

[11] I. Tien, S. D. Glaser, D. S. Goodin, and M. J. Aminoff, "Results of using a wireless inertial measuring system to quantify gait motions in control subjects," *IEEE Trans. Biomed. Eng.*, vol. 14, no. 4, pp. 904–915, Jul. 2010.

[12] A. Sabatini, C. Martelloni, S. Scapellato, and F. Cavallo, "Energy expenditure rate in level and uphill treadmill walking determined from empirical models and foot inertial sensing data," *IET Electron. Lett.*, vol. 40, pp. 95–96, Jan. 2004.

[13] S. P. Kwakkel, G. Lachapelle, and M. E. Cannon, "GNSS aided in situ human lower limb kinematics during running," in *Proc. ION GNSS*, Savannah, GA, Sep. 2008.

[14] S. Kwakkel, S. Godha, and G. Lachapelle, "Foot and ankle kinematics during gait using foot mounted inertial system," in *Proc. ION 2007 Nat. Tech. Meeting*, San Diego, CA, Jan.

[15] I. Skog, J. Nilsson, and P. Händel, "Evaluation of zero-velocity detectors for foot-mounted inertial navigation systems," in *Proc. 2010 Int. Conf. Indoor Positioning and Indoor Navigation*, Zurich, Switzerland, Sep.2010.

[16] N. El-Sheimy and X. Niu, "The promise of MEMS to the navigation community," *InsideGPS*, vol. 2, pp. 46–56, Mar./Apr. 2007.

[17] I. Skog and P. Händel, "In-car positioning and navigation technologies—A survey," *IEEE Trans. Intell. Transp. Syst.*, vol. 10, no. 1, pp. 4–21, Mar. 2009.

[18] D. Roetenberg, P. Slycke, and P. H. Veltink, "Ambulatory position and orientation tracking fusing magnetic and inertial sensing," *IEEE Trans. Biomed. Eng.*, vol. 54, no. 5, pp. 883–890, May 2007.

[19] A. M. Sabatini, "Quaternion-based extended Kalman filter for determining orientation by inertial and magnetic sensing," *IEEE Trans. Biomed. Eng.*, vol. 53, no. 7, pp. 1346–1356, Jul. 2006.

[20] P. H. Veltink, H. B. Bussmann, W. de Vries, W. L. Martens, and R. C. Van Lummel, "Detection of static and dynamic activities using uniaxialaccelerometers," *IEEE Trans. Rehabil. Eng.*, vol. 4, no. 4, pp. 375–385, Dec. 1996.

[21] S. Godha, G. Lachapelle, and M. E. Cannon, "Integrated GPS/INS system for pedestrian navigation in a signal degraded environment," in *Proc. ION GNSS*, Fort Worth, TX, Sep. 2006.

[22] B. Krach and P. Robertson, "Integration of foot-mounted inertial sensors into a bayesian location estimation framework," in *Proc. 5th Workshop Positioning, Navigat. Comm.*, Hannover, Germany, Mar. 2008.

[23] S. M. Kay, *Fundamentals statistical signal processing, detection theory*. Englewood Cliffs, NJ: Prentice-Hall, 1993.

[24] D. H. Titterton and J. L. Weston, *Strapdown Inertial Navigation Technology*, 2nd ed., The Institute of Electrical Engineering, Herts, U.K., 2004.

[25] K. R. Britting, *Inertial Naviagtion Systems Analysis*. New York: Wiliy-Interscience, 1971.

[26] I. Skog and P. Händel, "Calibration of a MEMS inertial measurement unit," presented at the XVII IMEKO World Congr., Rio de Janeiro, Brazil, Sep. 2006.

[27] A. M. Sabatini, "Quaternion-based strap-down integration method for applications of inertial sensing to gait analysis," *Med. Biol. Eng. Comput.*, vol. 43, pp. 94–101, Feb. 2005.

[28] S. M. Kay, *Fundamentals of Statistical Signal Processing, Estimation Theory*. Englewood Cliffs, NJ: Prentice-Hall, 1993.

[29] F. Cavallo, A. M. Sabatini, and V. Genovese, "A step toward GPS/INS personal navigation systems: Real-time assessment of gait by foot inertial sensing," in *Proc. Int. Conf. Intell. Robots Syst.*, Edmonton, AB, Canada, Aug. 2005.

[30] J. M. Hausdorff, Z. Ladin, and J. Y. Wei, "Footswitch system for measurement of the temporal parameters of gait," *J. Biomech.*, vol. 28, no. 3, pp. 347–351, 1995.

[31] T. Fawcett, "An introduction to ROC analysis," *Pattern Recognit. Lett.*, vol. 27, pp. 861–874, Jun. 2006.

Isaac Skog (S'09–M'10) received the B.Sc., M.Sc., and Ph.D. degrees in electrical engineering, wireless systems, and signal processing from the Royal Institute of Technology, Stockholm, Sweden, in 2003, 2005, and 2010, respectively.

During the spring of 2009, he was a Visiting Researcher at the Mobile Multisensor System Research Team, University of Calgary, Canada. He is currently a Postdoctoral Fellow at the Signal Processing Laboratory, Royal Institute of Technology. His research interests include signal processing and estimation theory with applications to low-cost navigation solutions.

Peter Händel (S'88–M'93–SM'98) received the M.Sc. and Ph.D. degrees from Uppsala University, Uppsala, Sweden, in 1987 and 1993, respectively.

From 1987 to 1993, he was at various positions at Uppsala University. During 1993 through 1997, he was with Ericsson AB, Kista, Sweden. During 1996 and 1997, he was a Visiting Scholar with the Signal Processing Laboratory, Tampere University of Technology, Finland. Since 1997, he has been with the Royal Institute of Technology, Stockholm, Sweden, where he is currently a Professor of signal processing. He has been engaged as an Associate Editor of the IEEE TRANSACTIONS ON SIGNAL PROCESSING.

John-Olof Nilsson received the M.Sc. degree in applied physics from Royal Institute of Technology, Stockholm, Sweden, in 2008, where he is currently working toward the Ph.D. degree in signal processing from the Signal Processing Laboratory.

His current research interests include signal processing, estimation theory, and implementation issues within aided inertial navigation.

Jouni Rantakokko received the M.Sc. degree in electrical engineering from the Royal Institute of Technology, Stockholm, Sweden, in 1998.

Since 1998, he has been employed at the Swedish Defense Research Agency (FOI), Linköping, Sweden, where he is currently a Senior Researcher and a Project Manager for research projects targeting tactical communications and robust indoor positioning systems. His research interests include adaptive antenna arrays, intersystem interference, adaptive link-layer techniques, multiple-input–multiple-output systems, and radio-based positioning.